Semi-convective planetary cores: the oscillatory instability

Sonja Zhou Wahlgren

PhD supervised by Alexandre Fournier & Thomas Gastine

May 23, 2025

IPGP
Université Paris Cité

Planets and semi-convection

- New data from space missions Juno and Cassini for Jupiter and Saturn

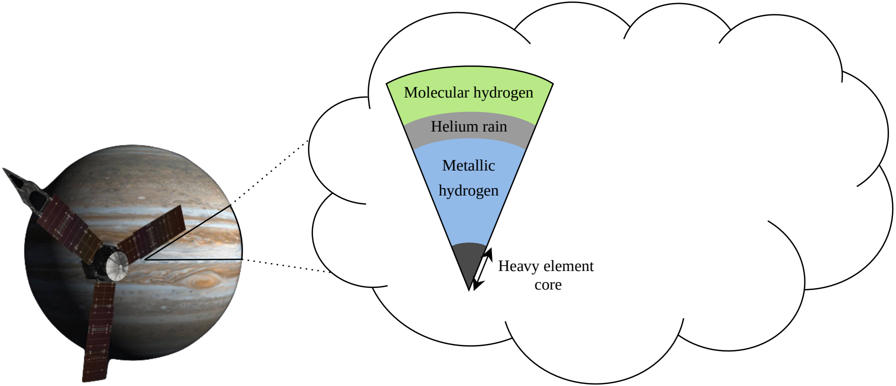

https://www.nasa.gov/mission_pages/juno/images/index.html

Planets and semi-convection

- New data from space missions Juno and Cassini for Jupiter and Saturn
- Existence of a dilute core

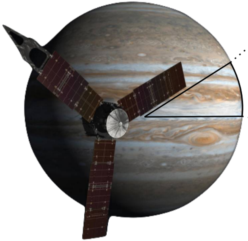

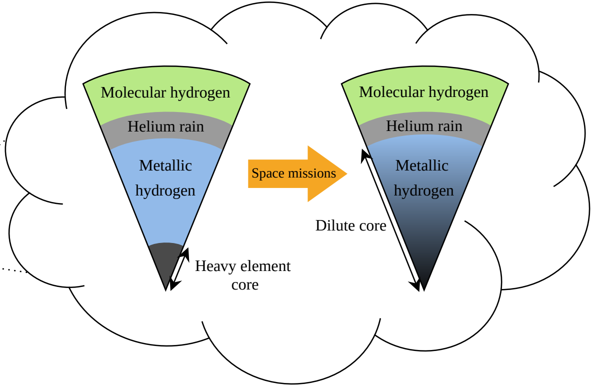

https://www.nasa.gov/mission_pages/juno/images/index.html

Planets and semi-convection

- New data from space missions Juno and Cassini for Jupiter and Saturn
- Existence of a dilute core
- Stabilising $\nabla\xi$ vs. destabilising ∇T

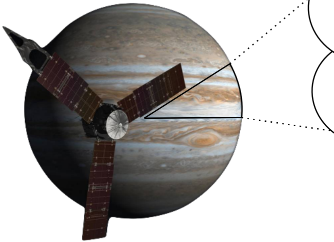

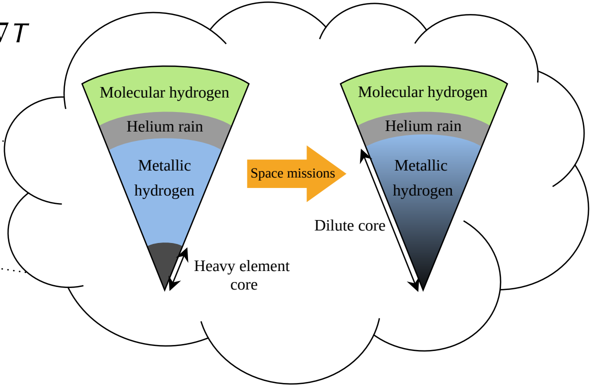

https://www.nasa.gov/mission_pages/juno/images/index.html

Previous studies

- Density ratio is a key parameter:

$$R_\rho = \frac{\alpha_T}{\alpha_\xi}\left|\frac{\nabla T}{\nabla \xi}\right| \tag{1}$$

- Linear stability threshold at $R_{\rho,c}^{-1}$ (Veronis, 1965)
- Regimes found in Cartesian geometry:

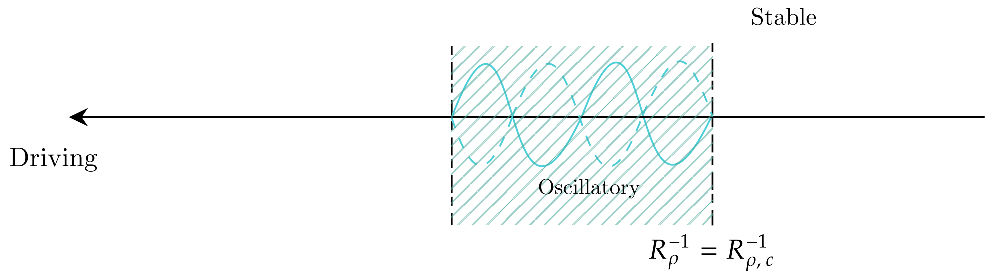

Previous studies

- Density ratio is a key parameter:

$$R_\rho = \frac{\alpha_T}{\alpha_\xi}\left|\frac{\nabla T}{\nabla \xi}\right| \quad (1)$$

- Linear stability threshold at $R_{\rho,c}^{-1}$ (Veronis, 1965)
- Regimes found in Cartesian geometry:

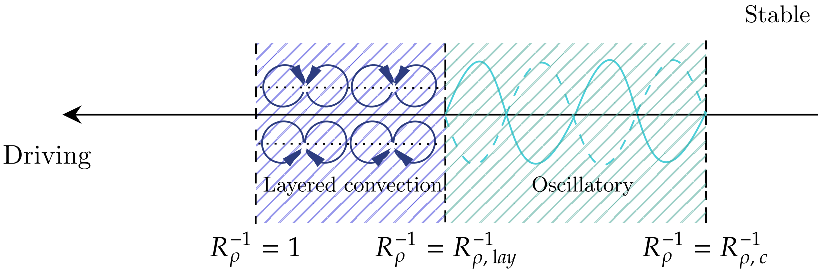

Figure adapted from Mirouh et al. (2011)

Previous studies

- Density ratio is a key parameter:

$$R_\rho = \frac{\alpha_T}{\alpha_\xi}\left|\frac{\nabla T}{\nabla \xi}\right| \quad (1)$$

- Linear stability threshold at $R_{\rho,c}^{-1}$ (Veronis, 1965)
- Regimes found in Cartesian geometry:

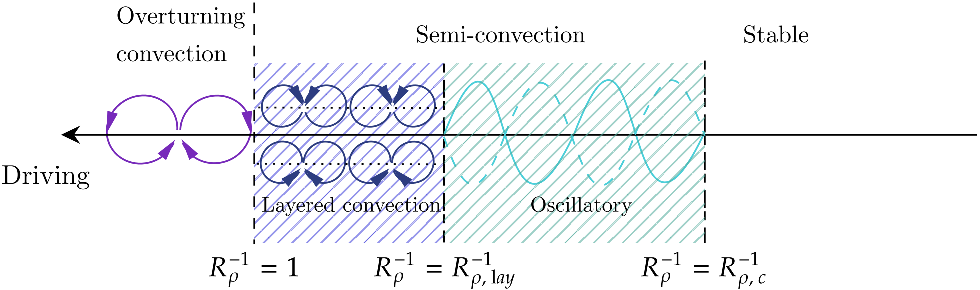

Figure adapted from Mirouh et al. (2011)

Goals of the work: global spherical study

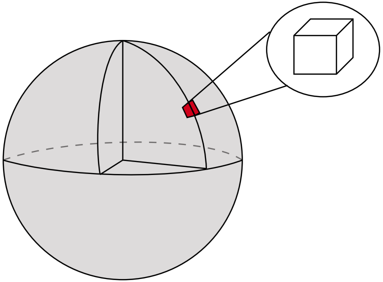

In which regions of parameter space do semi-convective instabilities develop and could they exist in planets such as Jupiter or Saturn?

Are the results from previous studies corroborated in this global geometry?

Model and parameters

Model:

- Conservation of mass, momentum, heat and composition
- Non rotating sphere
- Boussinesq approximation:

$$\rho = \rho_b[1 - \alpha_T(T - T_0) - \alpha_\xi(\xi - \xi_0)]$$

Numerics:

- 94 numerical simulations performed on S-CAPAD, IPGP
- Open-source code MagIC [a]

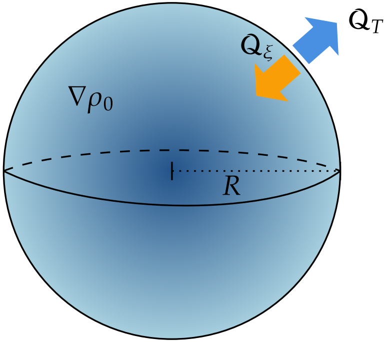

a. https://github.com/magic-sph/magic

Internal Gravity Modes (IGM)

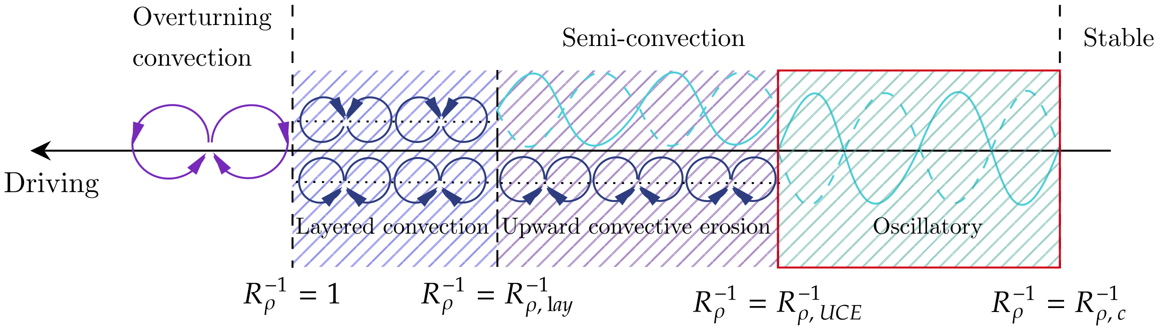

Internal Gravity Modes

- Fluid parcels oscillates at the Brunt-Väisälä frequency N

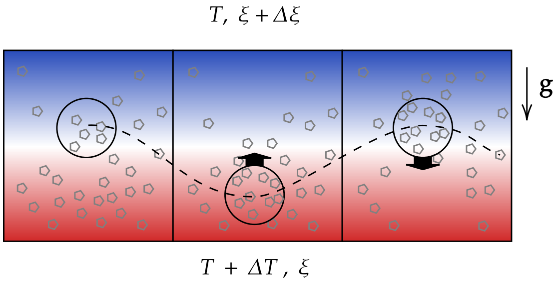

- Waves often found in natural systems such as oceans, atmosphere and planetary systems

Picture from https://user.eumetsat.int/resources/case-studies/internal-waves-in-the-eastern-strait-of-gibraltar

Linear stability analysis: Onset mode

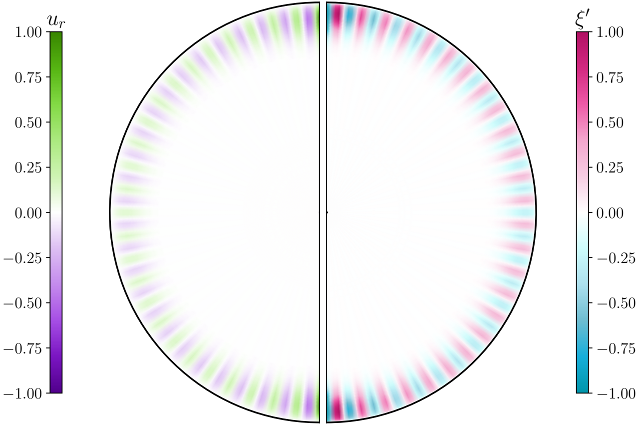

- Internal gravity modes
- Confined to outer fluid regions

Internal Gravity Modes (IGM)

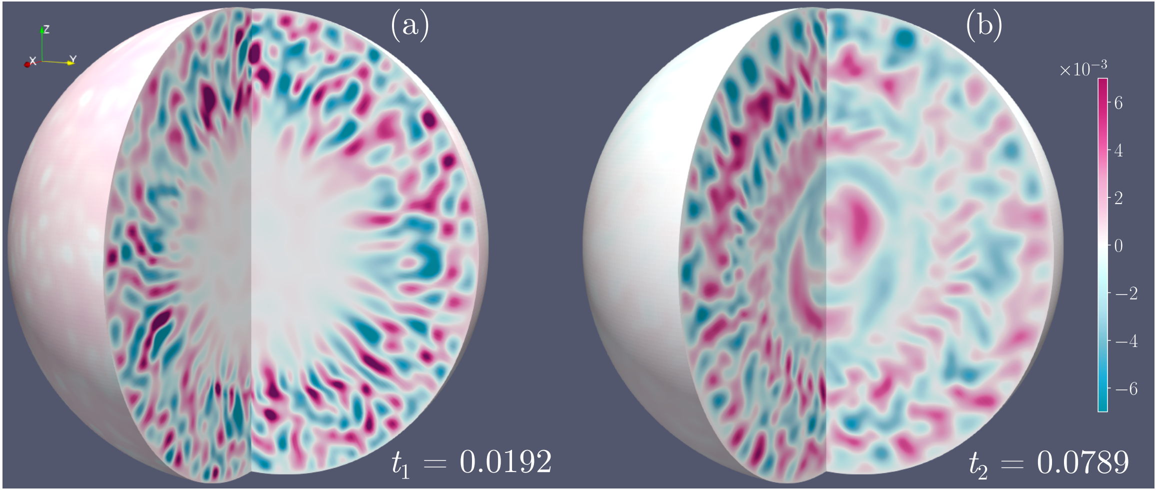

Characterisation of IGMs

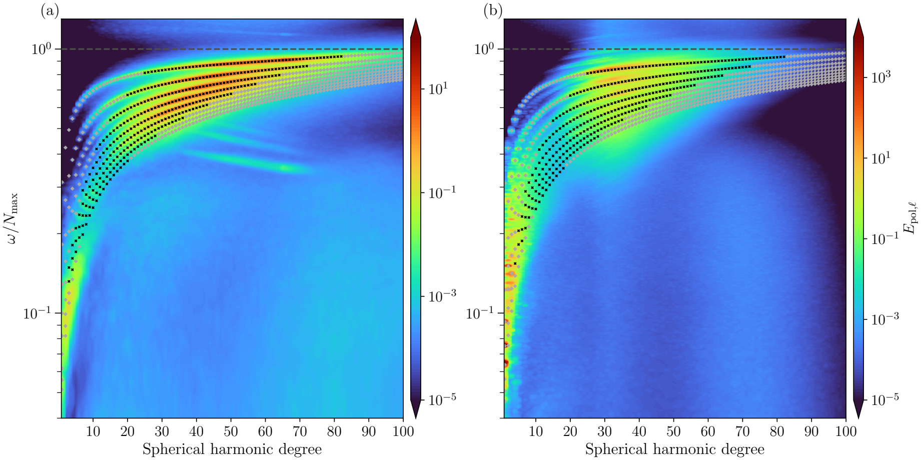

Characterisation of IGMs

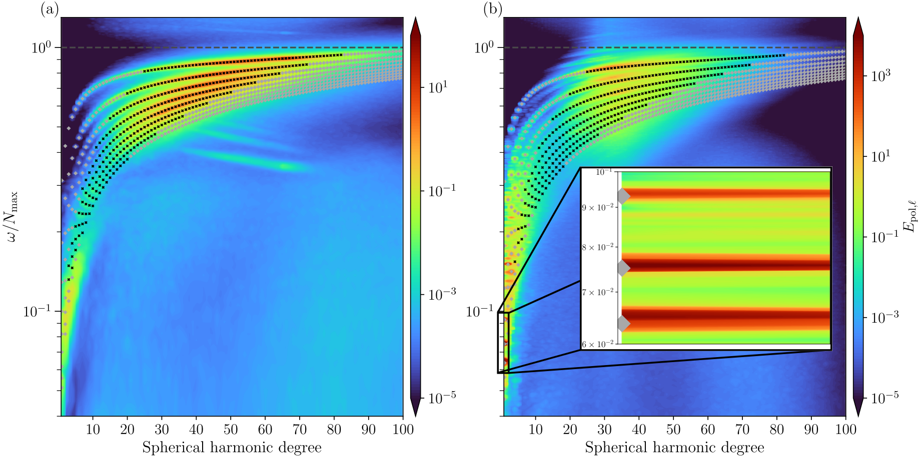

- Strongest contribution from $\ell = 1,\ n = 6$ ($\omega/N_{\max} = 0.07$)

Triadic resonance

- Eigenvalues of each mode given by $\lambda^k = \tau^k + i\omega^k$

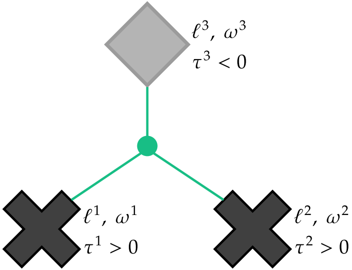

- Weakly nonlinear interactions can occur when $|\ell^1 - \ell^2| \leqslant \ell^3 \leqslant \ell^1 + \ell^2$
- Resonance condition: $|\omega^1 \pm \omega^2| = \omega^3$

Triadic resonance

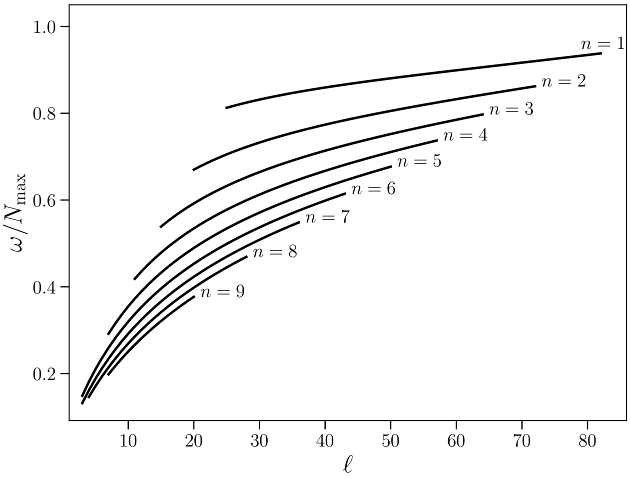

- Target mode $\omega^3_{1,6} = 0.07N_{\max}$ (most energetic)
- $(\ell^1 = 59, n = 1)$ and $(\ell^2 = 58, n = 2)$ have the strongest combined growth rates

Triadic resonance

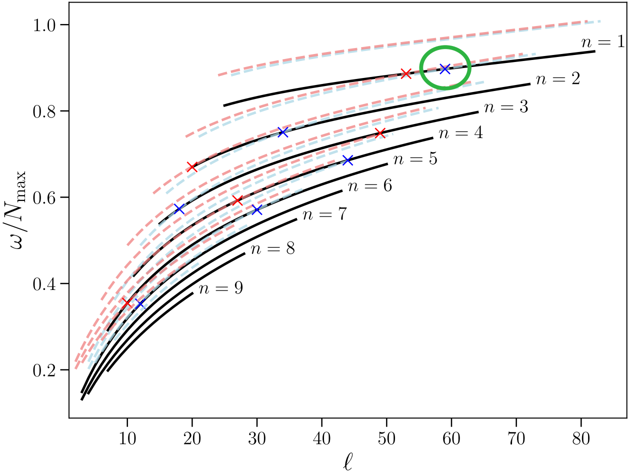

- Target mode $\omega^3_{1,6} = 0.07 N_{\max}$ (most energetic)
- $(\ell^1 = 59, n = 1)$ and $(\ell^2 = 58, n = 2)$ have the strongest combined growth rates

Triadic resonance

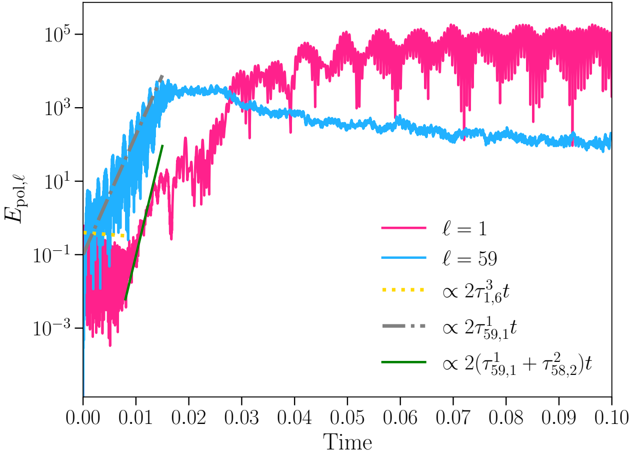

- Target mode $\omega^3_{1,6} = 0.07N_{\mathrm{max}}$ (most energetic)
- $(\ell^1 = 59, n = 1)$ and $(\ell^2 = 58, n = 2)$ have the strongest combined growth rates

Conclusion

- Characterisation the oscillatory regime
- Triadic resonance as a mechanism to explain the energy distribution

Ongoing work and perspective:

- Further analysis on other semi-convective regimes (Upward Convective Erosion, Layered convection)

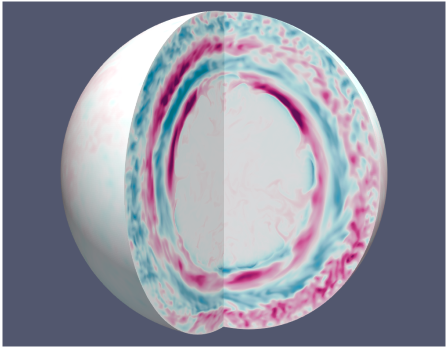

References I

- James, R. W. (1973). « The Adams and Elsasser Dynamo Integrals ». In: *Proceedings of the Royal Society of London. Series A, Mathematical and Physical Sciences* 331.
- Lago, R. et al. (2021). « MagIC v5.10: a two-dimensional MPI distribution for pseudo-spectral magneto hydrodynamics simulations in spherical geometry ». In: *Geoscientific Model Development* 14. DOI: 10.5194/gmd-14-7477-2021.
- Mirouh, G. et al. (2011). « A new model for mixing by double-diffusive convection (semi-convection): I. The conditions for layer formation ». In: *Astrophysical Journal* 750. DOI: 10.1088/0004-637X/750/1/61.
- Schaeffer, N. (Mar. 2013). « Efficient Spherical Harmonic Transforms aimed at pseudo-spectral numerical simulations ». In: *Geochemistry, Geophysics, Geosystems* 14. DOI: 10.1002/ggge.20071.

References II

- Valdettaro, L. et al. (2007). « Convergence and round-off errors in a two-dimensional eigenvalue problem using spectral methods and Arnoldi-Chebyshev algorithm ». In: *Journal of Computational and Applied Mathematics* 205, pp. 382–393. DOI: 10.48550/arXiv.physics/0604219.
- Veronis, G. (1965). « On finite amplitude instability in thermohaline convection ». In: *Journal of Marine Research* 23.1, pp. 1–17.
- Wicht, J. (2002). « Inner-core conductivity in numerical dynamo simulations ». In: *Physics of the Earth and Planetary Interiors* 132.4, pp. 281–302. DOI: https://doi.org/10.1016/S0031-9201(02)00078-X.

Appendix 1: Governing equations

$$
\begin{aligned}
\nabla \cdot \mathbf{u} &= 0 \, , \\
\frac{\partial \mathbf{u}}{\partial t} + (\mathbf{u} \cdot \nabla)\mathbf{u} &= -\nabla p' + \nabla^2 \mathbf{u} + \frac{Ra_T}{Pr} \left(T + R_\rho^{-1} \xi \right) g \mathbf{e}_r \, , \\
Pr \left[\frac{\partial T}{\partial t} + (\mathbf{u} \cdot \nabla) T \right] &= \nabla^2 T + S_T \, , \\
PrLe \left[\frac{\partial \xi}{\partial t} + (\mathbf{u} \cdot \nabla) \xi \right] &= \nabla^2 \xi + S_\xi \, ,
\end{aligned}
$$

where

$$
Ra_T = \frac{\alpha_T g_0 Q_T R^4}{\kappa_T^2 \nu \rho c_p} \, , \quad Pr = \frac{\nu}{\kappa_T} \, , \quad Le = \frac{\kappa_T}{\kappa_\xi} \, , \quad R_\rho^{-1} = Le c_p \frac{\alpha_\xi Q_\xi}{\alpha_T Q_T}
$$

Appendix 2: Numerical method

- Finite difference radial scheme, spherical harmonic expansion in the horizontal direction
- IMEX time scheme of order 3
- Open source high-performance code MagIC [1] (Wicht, 2002; Lago et al., 2021) with the SHTns library [2] (Schaeffer, 2013)
- 94 simulations on S-CAPAD/DANTE, initialised with random noise on a conductive state
- $Pr = 0.3$ and $Le = 10$, varying Ra_T and $1 < R_\rho^{-1} < 3.25$ (Veronis, 1965)
- Linear Solver Builder to treat the linear problem (Valdettaro et al., 2007)

1. https://github.com/magic-sph/magic
2. https://gricad-gitlab.univ-grenoble-alpes.fr/schaeffn/shtns

Appendix 3: Resonance and nonlinear interaction

- Resonance conditions:

$$|\omega^1 \pm \omega^2| = \omega^3$$

- Nonlinear interaction of IGMs in a non-rotating spherical geometry (James, 1973):

$$m^1 + m^2 + m^3 = 0 \, ,$$
$$\ell^1 + \ell^2 + \ell^3 \quad \text{is even,}$$
$$|\ell^1 - \ell^2| \leqslant \ell^3 \leqslant \ell^1 + \ell^2 \, .$$

Appendix 4: Diffusivity-free limit

- Diffusivity-free vs exact eigenfunction
- Left: $Ra_T = 10^7$, $R_{\rho,c}^{-1} = 2.69$, $\ell_c = 15$
- Right: $Ra_T = 10^9$, $R_{\rho,c}^{-1} = 2.992$, $\ell_c = 52$

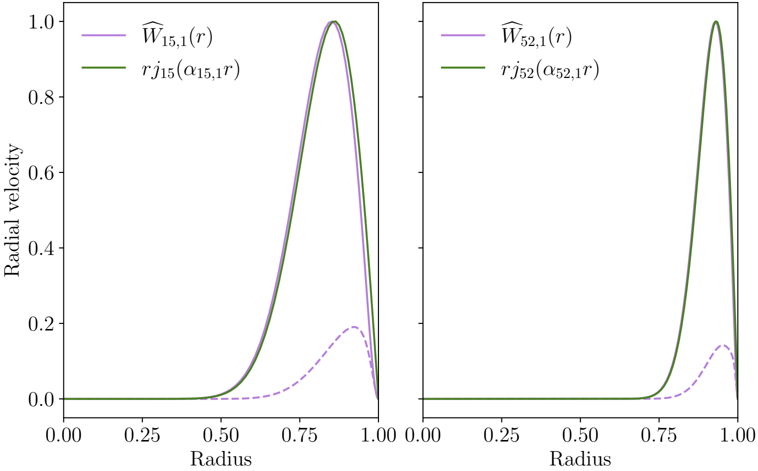

Appendix 5: Merging rate

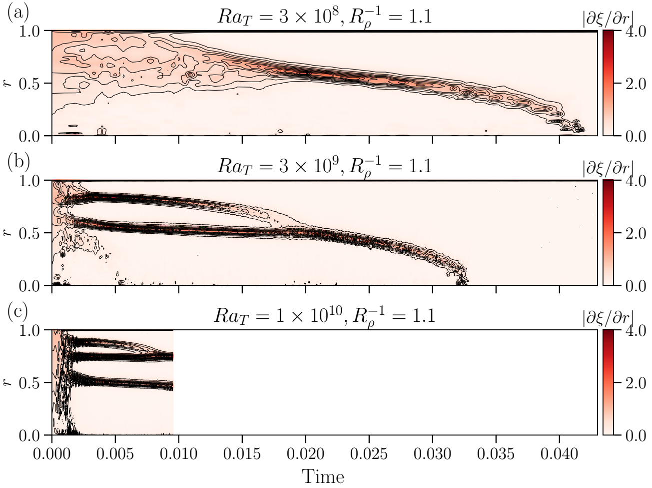

- (a) $t_{\text{lay}} \sim 0.04\tau_\nu$
- (b) $t_{\text{lay1}} \sim 0.017\tau_\nu$, $h_{\text{lay1}} \sim 0.2$
  $t_{\text{lay2}} \sim 0.032\tau_\nu$, $h_{\text{lay2}} \sim 0.4$
- (c) $t_{\text{lay1}} \sim 0.006\tau_\nu$

➤ τ_ν not the relevant time scale

Appendix 6: IGM, different fields

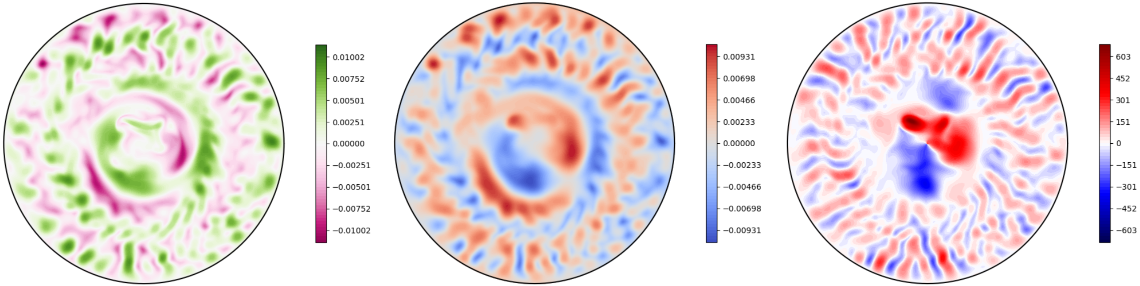

(a) ξ fluctuations (b) T fluctuations (c) u_r

Appendix 7: UCE, different fields

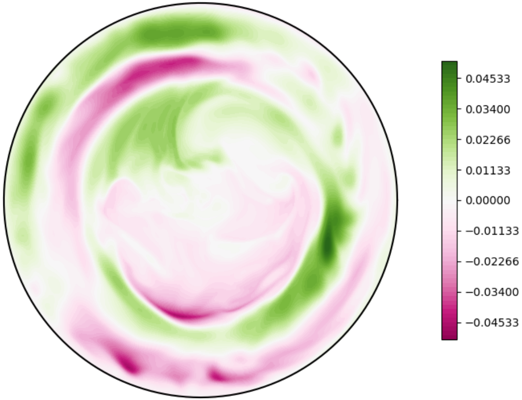

(a) ξ fluctuations

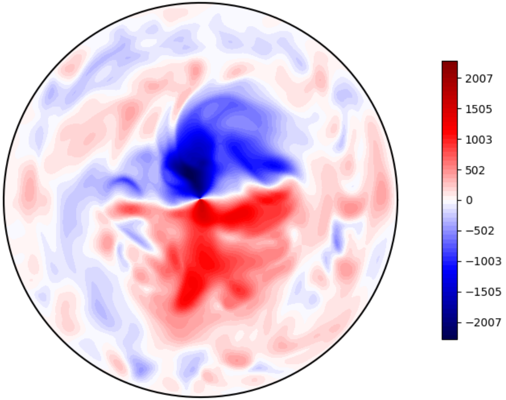

(b) u_r

Appendix 8: LC, differents fields

(a) ξ (b) ξ fluctuations (c) u_r

Appendix 9: LC, animation